(Received 8 December 2023, Accepted 18 January 2024, Scheduled 29 January 2024)

RIS-Assisted Wireless Channel Characteristic in Coal Mine Tunnel Based on 6G Mobile Communication System

Shuqi Wang* and Wei Zhang

School of Communication and Information Engineering
Xi'an University of Science and Technology, Xi'an 710054, Shaanxi, China

ABSTRACT: In the context of 6G communication technology, Reconfigurable Intelligent Surfaces (RIS) can effectively reconfigure signal propagation paths through the adjustment of their passive metamaterial reflector units. This capability mitigates the issue of radio wave attenuation in the complex environments of mine tunnels by optimizing signal paths, thereby reducing energy loss and minimizing coverage dead zones. By utilizing RIS-assisted multi-antenna terrestrial mobile communication channels and ray tracing techniques, researchers have established a wireless channel fading model specifically for rectangular coal mine tunnels. The results suggest that under comparable conditions, RIS technology enhances low-frequency signals (e.g., 2.4 GHz) more effectively than high-frequency signals (e.g., 30 GHz). Furthermore, these improvements are more pronounced as the size of the RIS increases.

1. INTRODUCTION

The communication systems in coal mine tunnel are often severely impacted by multipath interference, electrical noise, coal-rock dielectric constant, and absorption of propagation medium, which greatly restrict the real-time transmission and processing capabilities of underground information. As a vanguard innovation in the sphere of 6G telecommunications, the concept of RIS (Reconfigurable Intelligent Surfaces) [1–4] has been posited for integration within subterranean communication networks. This integration aims to optimize the information transmission and blind spot coverage of the coal mine tunnel. The hardware construction of RIS is based on a metasurface, comprising an electrolytic substrate and copper plate, and incorporates a planar array of sub-wavelength tunable passive reflector units. These units are externally manipulated in amplitude and phase by an intelligent controller (e.g., FPGA: field programmable gate array) [4]. The reflector units, composed of PIN diodes and load resistors, generate phase shifts through the switching states of the diodes. The controller adjusts the signal phase by setting different bias voltages, while load resistors with varying resistances are employed to modify the signal amplitude.

Currently, extensive research has delved into various aspects of RIS in ground-space channels, including theoretical analysis of RIS channels [5], estimation of achievable rates in RIS-assisted communication systems [6], maximization of energy efficiency in RIS-aided downlink systems [7], as well as the optimization of energy harvesting performance, spectral efficiency, bit error rate, and outage probability in RIS-assisted wireless communications [8]. In the study of RIS channel modeling and wave loss characteristics, the authors in [9] concentrated on the physical channel modeling of RIS-assisted wireless networks within the Sub-6 GHz band. The study takes into account both far-field and near-field transmission behaviors, and proposes an open-source physical channel simulator. This simulator is adaptable in terms of operating frequency, propagation environment, terminal locations, as well as the size and position of the RIS. The authors in [10] conducted multi-scenario broadband channel measurements and modeling in the Sub-6 GHz band, encompassing outdoor, indoor, and outdoor-to-indoor environments. The study introduced two improved empirical models and analyzed the propagation characteristics of RIS-assisted channels, such as path loss gain, spatial consistency, and frequency stability.

In terms of channel transmission performance, the authors in [11] analyzed the performance of RIS channels under both static and dynamic scenarios, considering Rayleigh fading and Additive Generalized Gaussian White Noise (AAGWN). It also derives closed-form expressions for the average Bit Error Rate (BER), average Channel Capacity (ACC), and Outage Probability (OP) in these two scenarios. The challenges of channel estimation and the impact of feedback overhead in RIS-assisted systems are also under investigation. In the context of Orthogonal Frequency Division Multiplexing (OFDM) systems assisted by RIS, the authors in [12] and [13] introduced a transmission protocol that sequentially carries out channel estimation and reflection optimization. This protocol employs a low-complexity algorithm based on the strongest signal in the time domain to optimize the reflection coefficients after estimating the Channel State Information (CSI). This approach enhances the efficacy of the system's estimation methodology. However, the cost associated with estimating CSI was not considered. The authors in [14] addressed this gap by proposing an expression that combines an overhead model with energy efficiency and transmission rate. This expression is used for optimizing power and bandwidth during communication and feedback phases, maximizing a balance between resource allocation and overhead.

* Corresponding author: Shuqi Wang (wangshuqi@xust.edu.cn).

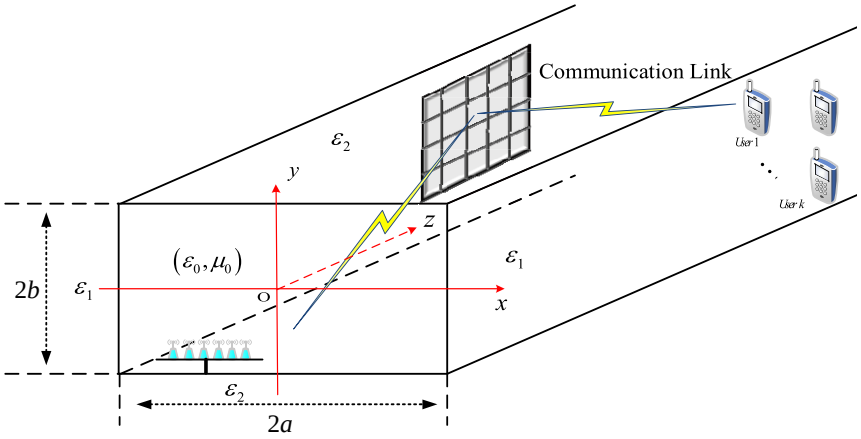

FIGURE 1. RIS-assisted underground rectangular tunnel communication system model.

RIS, as a passive reflective material, possesses the capability to actively control electromagnetic wave beams in wireless environments, enabling beamforming and lossless reflection. The authors in [15] provided a comprehensive overview of RIS design work from the perspectives of prototype system and unit design. They also categorized and reviewed channel modeling for RIS-assisted indoor communications. In the application of RIS in coal mines, the authors in [16] proposed an innovative method of using RIS technology to achieve wireless signal coverage and fill coverage gaps in mine channels. By strategically deploying RIS, the absorption and scattering of the main signal components by tunnel walls are reduced, and signal strength and coverage are enhanced through phase reconstruction. Building on this foundation, the study conducted a series of experiments to verify the effectiveness of RIS technology in specific underground mining environments. Utilizing Monte Carlo simulations for the RIS-augmented subterranean channel loss model, signal loss across 2.4 GHz, 5.8 GHz and 30 GHz bands is rigorously analyzed. The results show that RIS can greatly reduce the transmission loss of the signal in the tunnel, and this improvement is more obvious for the low-frequency signal. The loss of 2.4 GHz signal at 100 meters can be reduced by 54.78%, and 5.8 GHz signal loss can be reduced by 31.89%. In addition, for the high-frequency signal of 30 GHz, there is a threshold for the improvement characteristics of RIS, and when the transmission distance exceeds 100 meters, the improvement effect of RIS is not obvious, which puts forward a new possibility for the next stage of multiple RIS in the downhole to optimize the propagation of the signal. Moreover, enhancing the size of RIS markedly improved the power and reach of the transmitted signal. These findings not only validate RIS's role in elevating underground transmission quality and broadening coverage in signal-blind areas but also offer practical directives for designing subterranean communication systems, with substantial implications for safety and efficiency in coal mining operations.

The main contributions of this article can be summarized in three key aspects: (1) This study explores the application of Reconfigurable Intelligent Surface (RIS) technology in coal mine tunnels, which focuses on the modeling and analysis of the RIS channel matrix, as well as an analysis of coal mine tunnel noise. (2) A mine channel fading model assisted by RIS technology has been constructed and employs ray tracing methods to analyze propagation paths in rectangular tunnels, constructing an RIS channel fading model under rough loss conditions. (3) The paper elucidates how RIS decisively ameliorates the channel characteristics of mine communications, particularly in terms of mitigating signal attenuation. These analyses provide a detailed understanding of the impact of RIS on enhancing communication in challenging environments, underscoring its vital role in advancing mining communication systems.

The article is divided into five sections. The first is an introduction, outlining the research background and the application of RIS technology in mining. The second discusses RIS channel matrix modeling and coal mine noise analysis. The third section uses ray tracing to analyze tunnel propagation paths and construct an RIS channel fading model. The fourth section includes simulation experiments. The fifth concludes the paper.

2. SYSTEM MODEL

2.1. Channel Matrix Model

The RIS-assisted straight tunnel wireless communication system model is depicted in Figure 1, in which the Cartesian coordinate system is established at the center of cross-section of the tunnel, and the radio wave propagates along the axis direction. The RIS is positioned between the Base Station (BS) and User Equipment (UE), with their primary function being to enhance signal strength and extend propagation distance. It is assumed that the tunnel has a width of $2a$ and a height of $2b$, with both side walls as well as the top and bottom having a relative permittivity of ε_r. The interior of the tunnel is filled with an ideal transmission medium characterized by electrical parameters (ε_0, μ_0). The underground tunnel structure of coal mine is complex and diverse, which can be roughly divided into three typical application scenarios (I-type tunnel, L-shaped tunnel, and T-shaped tunnel) as shown in Figure 2. It should be noted that although there are three types of roadway structures, the channel matrix model assisted by RIS is consistent.

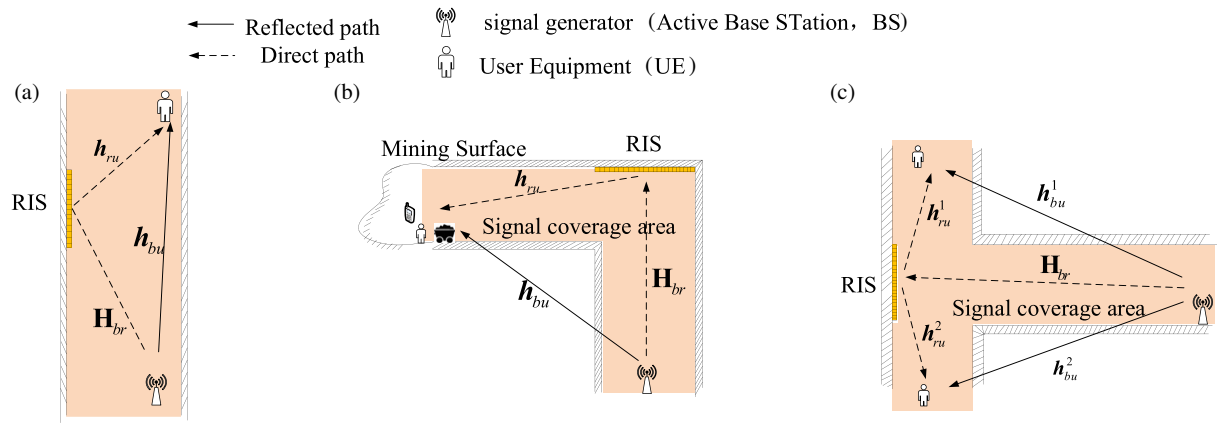

FIGURE 2. Underground deployment of RIS in (a) I-Type, (b) L-Type, and (c) T-Type scenarios.

In this model, when an electrical signal travels from the base station and reaches the RIS, it passes through multiple effective scattering paths, expressed as R_{br}. Each of these paths possesses a specific amplitude α_i (represented as the amplitude of the ith scattering path), delay τ_i (represented as the delay for the ith scattering path to reach the RIS unit), and phase ϕ_i (represented as the phase for the ith scattering path to reach the RIS unit). Here, $g_{br}(t)$ denotes the relationship between delay and phase. Therefore, the propagation model of the system's BS to RIS link can be described by these parameters:

$$g_{br}(t) = \sum_{i=0}^{R_{br}-1} \alpha_i \delta(t-\tau_i) e^{-j\phi_i} \quad i = 1, 2, \cdots, R_{br} \tag{1}$$

Converting Equation (1) into the frequency response of a narrowband system yields:

$$h(t) = \int_{-\infty}^{+\infty} g_{br}(t) e^{-j2\pi f_0 t} dt = \sum_{i=0}^{R_{br}-1} \alpha_i e^{-j2\pi f_0 \tau_i} e^{-j\phi_i} \tag{2}$$

In the wireless communication system under consideration, the radio wave signal finally received by the RIS is the vector sum of all signal rays emitted from the BS that are reflected multiple times through the reflector wall to reach the RIS. This signal reception mechanism is akin to the signal processing in Multiple-Input and Multiple-Output (MIMO) systems. In this context, for RIS reflective unit n, its channel coefficient can be expressed as per Equation (3). This channel coefficient collectively reflects the impact of all ray paths from the BS to that particular RIS unit, including the amplitude, phase, and delay characteristics of each path. This approach enables precise analysis and design of RIS-assisted wireless communication systems, optimizing the transmission and reception quality of the signal.

$$h_{nm}(t) = \sum_{i=0}^{R_{br}-1} \alpha_i e^{-j\frac{2\pi L_i^{BS-RIS}}{\lambda}} e^{-j\phi_i} \tag{3}$$

h_{nm} represents the channel impulse response between the transmitting antenna T_m and RIS unit R_n, while i denotes the number of transmission paths. Therefore, the BS-RIS channel matrix is defined as:

$$\mathbf{H}_{br} = \begin{bmatrix} H_{11} & H_{12} & \cdots & H_{1M} \\ H_{21} & H_{22} & \cdots & H_{2M} \\ \vdots & \vdots & & \vdots \\ H_{N1} & H_{N2} & \cdots & H_{NM} \end{bmatrix}_{N\times M} \in \mathbb{C}^{N\times M} \tag{4}$$

Similarly, the communication channel coefficient from RIS to UE is represented as:

$$\begin{aligned} h_{nu}(t) &= \int_{-\infty}^{+\infty} g_{nu}(t) e^{-j2\pi f_0 t} dt \\ &= \sum_{n=0}^{N-1} \beta_n e^{-j\frac{2\pi L_i^{RIS-UE}}{\lambda}} e^{-j\phi_n} \end{aligned} \tag{5}$$

Assuming that the UE is a single-antenna device, the channel matrix of the RIS-UE can be represented as a vector $\mathbf{h}_{nu}$ of dimension $\mathbb{C}^{N\times 1}$:

$$\mathbf{h}_{nu} = [h_{11} \;\; h_{21} \;\; \cdots \;\; h_{N1}]^T \in \mathbb{C}^{N\times 1} \tag{6}$$

In the RIS-assisted communication link, the reflective characteristics of the RIS units lie in their ability to modulate the amplitude and phase of the incident waves. The phase of the RIS reflection coefficient is represented as $\boldsymbol{\theta} = [\theta_1, \theta_2, \cdots, \theta_N]^T$, $\theta_n \in [0, 2\pi)$, and the amplitude is represented as $\boldsymbol{\beta} = [\beta_1, \beta_2, \cdots, \beta_N]^T$, $\beta_n \in [0, 1]$. Defining $\Phi_n = \beta_n e^{j\theta_n}$ as the reflection coefficient of the ith reflective unit, which includes the phase adjustment value for each unit, the RIS reflection coefficient matrix is represented as:

$$\boldsymbol{\Theta} = \text{diag}\left(\beta_n e^{j\theta_n}\right), \quad \theta_n \in [0, 2\pi) \tag{7}$$

Under the assumption that each unit of the RIS can reflect electromagnetic wave signals and that each reflective unit has the same amplitude $\beta \in [0, 1]$, the cascaded channel under RIS assistance is represented as $\mathbf{H}_{br}^H \boldsymbol{\Theta} \mathbf{h}_{nu}$. For Type I straight tunnel, considering the line-of-sight (LOS) link between the transmitter and receiver, the LOS path channel vector is defined as $\mathbf{h}_{bu} = [h_1^{bu} \;\; h_2^{bu} \;\; \cdots \;\; h_M^{bu}]^T \in \mathbb{C}^{M\times 1}$. Therefore, the combined signal matrix model for the direct link and the cascaded link is: $\mathbf{H}_{br}^H \boldsymbol{\Theta} \mathbf{h}_{nu} + \mathbf{h}_{bu}$.

2.2. Noise Factor Correction

Different from ground noise, the noise inside the coal mine tunnel is mainly reflected in the characteristics of the sound source, sound wave propagation path, and sound field environment. Noise inside the mine is mainly due to activities such as mechanical operations, drilling processes, and rock crushing inside the mine. The sound waves generated by these activities propagate through the narrow, enclosed space of the tunnel, and are reflected and refracted many times, increasing the noise level and complexity. Therefore, the Gaussian distribution is used to describe the sound sources generated by mechanical operation. Considering some sudden noises (such as equipment failure, etc.), this noise generation is regarded as a "Bernoulli experiment", i.e., random events that occur or do not occur. Therefore, a Gauss-Bernoulli distribution can be used to better describe the noise characteristics of the coal mine tunnel.

If the BS emits a signal $s(t)$, then the transmitted power is P_T. Define the weight vector of the sender antenna as $\boldsymbol{\omega}$, where $\boldsymbol{\omega} \in \mathbb{C}^{M\times 1}$ and is unit-modulus, meaning that each element of $\boldsymbol{\omega}$ has an absolute value of $\|\boldsymbol{\omega}\| = 1$. This ensures that the power of the reflected signal is conserved. Therefore, the expression for the received signal is:

$$y = \sqrt{P_T}\left(\mathbf{H}_{br}^H \boldsymbol{\Theta} \mathbf{h}_{nu} + \mathbf{h}_{bu}\right)^H \cdot \boldsymbol{\omega} \cdot s + n \tag{8}$$

n is the electrical noise of the mine, and due to the wide spectrum characteristics of the electrical noise, the electrical noise that affects the radio signal can be regarded as an impulse interference response. Therefore, we represent the signal noise in the underground roadway as:

$$n = \nu + \kappa \tag{9}$$

where ν represents the additive Gaussian white noise, and κ represents the impulse interference noise signal, $\kappa = \mathbf{B} \cdot \mathbf{G}$. In this equation, $\mathbf{B}$ is the Bernoulli distribution with a mean of 0, and a variance of success is 1. If the probability of success is p, it can be expressed as equation $\mathbf{B} \sim Bernoulli(p)$. If $\mathbf{G}$ is a Gaussian distribution that obeys $(0, 2\sigma^2)$, the downhole noise interference can be regarded as an independent and identically distributed Bernoulli-Gaussian process, which is expressed as:

$$n = \nu + \mathbf{B} \cdot \mathbf{G} \tag{10}$$

The noise power is expressed as:

$$P_{noise\_total} = \begin{cases} \sigma^2 + 2\sigma^2 p, & P = p \\ \sigma^2 + 2\sigma^2(1-p), & P \neq p \end{cases} \tag{11}$$

3. LOSS CHARACTERISTICS OF RIS AUXILIARY MINE RADIO WAVES

3.1. Analysis of Radio Wave Propagation Path Based on the Tent Law

In the underground tunnel environment, the electromagnetic wave signal emitted by the BS undergoes multiple reflections, and the spiral ray path [17] formed in the space limited by the four walls is particularly critical. In order to further study this complex reflection mechanism, a single ray emitted from the source was selected as the object of analysis, and the law of reflection in optics was applied, which can be divided into two different types of reflective surfaces: horizontal and vertical [18]. According to the "Tent second law" in geometrical optics, that is, when a ray is emitted at a specific starting point (point source: S), it will exist in both a horizontal and a vertical plane of incidence and will be reflected and propagate along the intersection of these two planes according to the law of reflection. In the transmission link from the BS to the RIS, if the number of reflections of the signal in the tunnel is M, the total number of valid paths to the RIS formed by the multiple reflections of the signal through the tunnel wall is a deterministic value and is expressed as [17]:

$$R_{br} = 2M^2 + 2M + 1 \tag{12}$$

According to the "Tent Third Law" [19], the length of a helical ray emanating from a transmission point S and reaching the receiver D after undergoing $m+n$ reflections off both the left and right walls, as well as the top and bottom plates, is equivalent to the linear distance covered by a mirrored image of point S, post $m+n$ reflections to the receiver. Consequently, the angle of arrival at the receiver is synonymous with the azimuth angle of this direct line.

To give a simple example, Figure 3 shows the propagation of a signal ray in a T-shaped roadway using the "Tent second law". The central axis of the precession is oriented along the z-axis, intersecting the horizontal plane at $(x_0, y_0, 0)$, where S is the emission point. The RIS is positioned at a certain point on the xy plane, denoted by P at Q, where the product of the horizontal coordinate $P \times Q = N$, P and Q are orthogonal coordinates. Additionally, the RIS central axis intersects the xy plane at a particular point, forming the RIS central axis' projected emission point (x_p, y_q, z).

Taking the depression angle as the observation direction in the three-dimensional coordinate system, the mirror point S^* of the point source S after $m+n$ reflection is found. Reference [20] informs us that by using the mathematical induction, it can be deduced that if the last reflection of the ray is on the right wall of the alleyway, the coordinates of the mirror image point after $m+n$ reflections are $S^m((2ma+(-1)^m x_0), y_0, 0)$. If it is stipulated that the last reflection of the signal occurs off the left alleyway wall, then by the same logic, the coordinates of the mirror image point after $m+n$ reflections are $S^m((-2ma+(-1)^m x_0), y_0, 0)$.

Summarizing the above can be summarized as:

$$S^*(x) = \begin{cases} 2ma + (-1)^m x_0, & \text{on the right wall} \\ -2ma + (-1)^m x_0, & \text{on the left wall} \end{cases} \tag{13}$$

In the same way, the coordinates of the mirror point reflected by $m+n$ times on the upper and lower walls can be expressed as:

$$S^*(y) = \begin{cases} 2nb + (-1)^n y_0, & \text{on the upper wall} \\ -2nb + (-1)^n y_0, & \text{on the lower wall} \end{cases} \tag{14}$$

When the rays are plucked in a rectangular tunnel, the coordinates of the mirror point through m horizontal mirrors

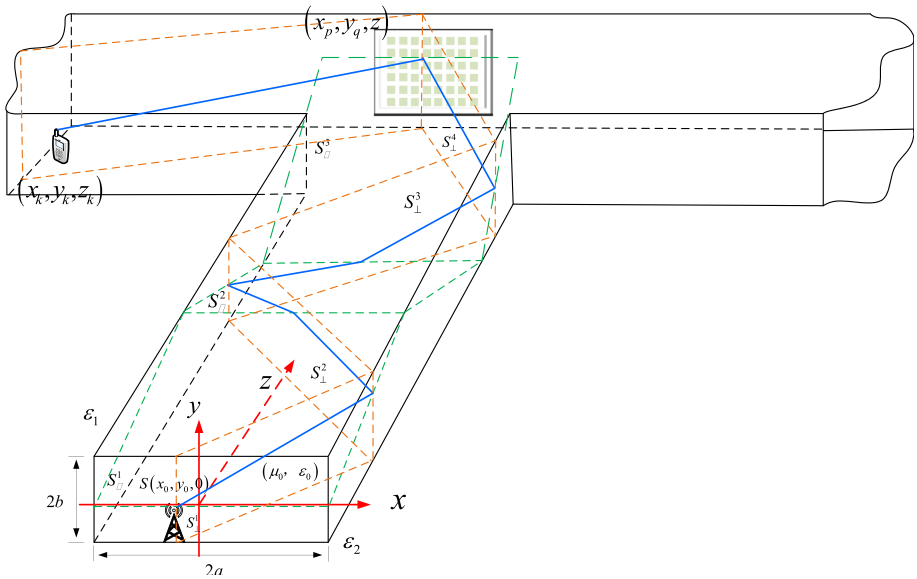

FIGURE 3. Schematic diagram of the second law of tents in a "T" shaped roadway.

and n vertical mirrors can be expressed as $S^*(S^*(x), y_0, 0)$ or $S^*(x_0, S^*(y), 0)$. Therefore, the length of the path for the rays emitted from an antenna of the Base Station to reach a certain unit (p, q) of the RIS through the tunnel wall reflection is calculated as:

$$\begin{aligned} d_{i,n} &= \sqrt{(S^*(x) - x_p)^2 + (y_0 - y_q)^2 + z^2} \\ d_{i,n} &= \sqrt{(x_0 - x_p)^2 + (S^*(y) - y_q)^2 + z^2} \end{aligned} \tag{15}$$

To concretize formula (15), the specific propagation path expression can be derived using mathematical induction, based on the reflection characteristic functions of the top and bottom plates and side walls. Assume that the height of the transmitting antenna above the ground is h_T; the height of the receiving antenna above the ground is h_R; the transmitting antenna is located at a distance g_T from the right wall; the receiving antenna is located at a distance g_R from the right wall; and the direct distance from the BS to a specific unit of the RIS transceiver is d. Because direct waves and reflected waves are the primary forms of transmission in the tunnel, we only study the effects of these two types of waves. The following Figure 4 illustrates the first reflection from the top and bottom plates and the first reflection from the sidewalls within the tunnel.

When the signal has undergone m reflections (m is an odd number), there is an $m+1$ segment polyline, which can be obtained by mathematical induction, and the mirror point of $m-1$ full roadway is required, then the path length of the single-hop odd reflection is calculated as:

$$L = \sqrt{[h_T + h_R + (m-1)H]^2 + d^2} \tag{16}$$

In the above formula, H represents the vertical distance between the walls or the roof and floor on both sides of the tunnel. When the angle between the ray and the roadway wall is expressed as θ, the incident angle can be calculated by $\theta_i = \pi/2 - \theta$, so the propagation angle relationship satisfies:

$$\sin\theta_i = \frac{d}{L}, \quad \cos\theta_i = \frac{h_T + h_R + (m-1)H}{L} \tag{17}$$

In the same way, for a single hop even number of reflections on a side wall of a tunnel, assuming that n reflections are made (n is an even number), there is an $n+1$ polyline, and the total path length obtained by mathematical induction is:

$$L' = \sqrt{[h_T - h_R + Hn]^2 + d^2} \tag{18}$$

Similarly, the angular relation satisfies:

$$\sin\theta_i = \frac{d}{L'}, \quad \cos\theta_i = \frac{h_T - h_R + Hn}{L} \tag{19}$$

3.2. Establishment of RIS-Assisted Rectangular Coal Mine Tunnel Radio Wave Loss Model

For the reflection loss of radio waves, the reflection coefficients defined as vertically polarized and horizontally polarized of radio waves on a smooth surface are as follows:

$$\begin{aligned} a_{\perp} &= \frac{\cos\theta_i - \sqrt{\varepsilon_r - \sin^2(\theta_i)}}{\cos\theta_i + \sqrt{\varepsilon_r - \sin^2(\theta_i)}}, \\ a_{\parallel} &= \frac{-\varepsilon_r\cos\theta_i + \sqrt{\varepsilon_r - \sin^2(\theta_i)}}{\varepsilon_r\cos\theta_i + \sqrt{\varepsilon_r - \sin^2(\theta_i)}} \end{aligned} \tag{20}$$

θ_i is the grazing angle of the ith path, and ε_r is the relative permittivity of the coal and rock. Assuming that the roughness obeys a mean of 0, a Gaussian distribution of variance h, and

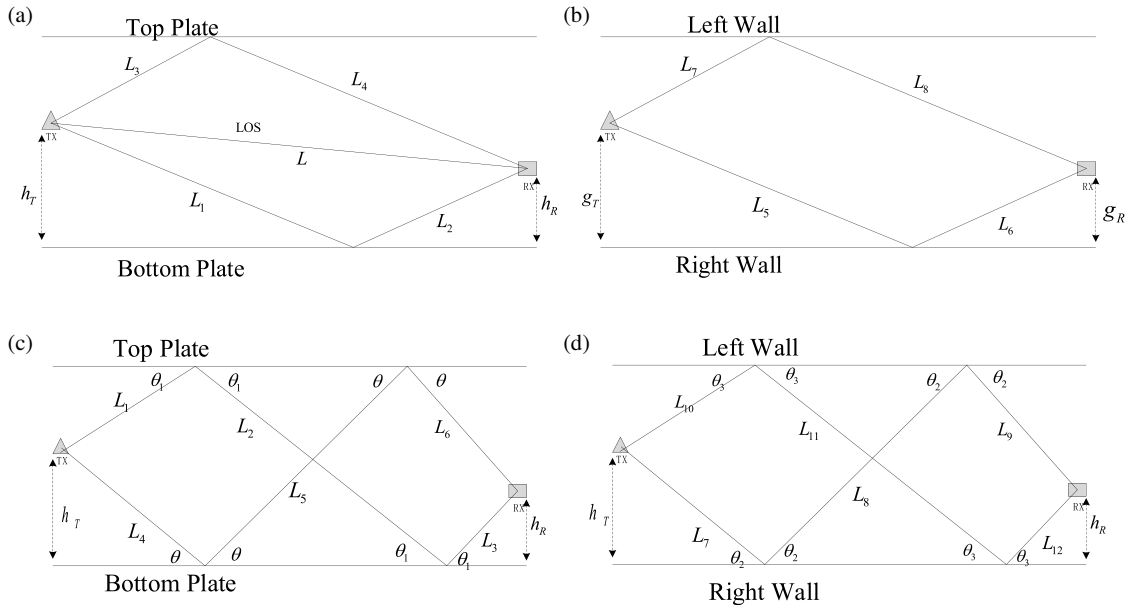

FIGURE 4. Primary and secondary reflection of the top and bottom plates and the walls on both sides [21].

$\rho_{roughness}$ denotes the roughness loss factor, then the scattering loss coefficient due to the rough surface is:

$$\rho_{\perp} = \rho_{roughness}\alpha_{\perp}, \quad \rho_{\parallel} = \rho_{roughness}\alpha_{\parallel} \tag{21}$$

$\rho_{roughness} = \exp\left(-8\left(\frac{\pi h \cos\theta_i}{\lambda}\right)^2\right)$ [14].

Therefore, the propagation loss of each ray reaching the receiving end can be obtained from the direct path loss and the reflection path loss in free space, which is expressed as:

$$P_r = P_t\left(\frac{\lambda}{4\pi L_{BS-RIS}}\right)^2\left(\frac{\lambda}{4\pi L_{RIS-UE}}\right)^2 G_t G_r G_{RIS} \tag{22}$$

G_{RIS} is the adjustable RIS gain, which is denoted as: $G_0(A_r/\lambda^2)N\cos^q\theta$. G_0 is the basic gain of each RIS unit, A_r the total effective area of the reflective surface, N the number of elements effectively participating in the reflection, and θ the angle of arrival of the electromagnetic wave. L_{BS-RIS} and L_{RIS-UE} indicate the path lengths on the BS-RIS and RIS-UE sides, respectively. Assuming that the fading of the downhole signal obeys the Rayleigh distribution, then its probability density function (PDF) is:

$$p(r) = \begin{cases} \frac{r}{\sigma^2}\exp\left(-\frac{r^2}{2\sigma^2}\right) & (0 \le r \le \infty) \\ 0 & (r < 0) \end{cases} \tag{23}$$

In the above equation, σ^2 represents the fading depth. $\Psi(r)$ is the fading loss factor of the Rayleigh distribution; L is the length of the reflection path; and in the RIS-UE link, L_{RIS-UE} is assumed to be the direct path after amplitude modulation and phase modulation. In addition, ξ_i represents the product of each reflection coefficient experienced by the ith path, and we take the calculation of the vertically polarized wave as an example, assuming that the rays are reflected m times on the walls on both sides and n times on the top and bottom plates, then the expression of the product of the reflection coefficient of a certain path i is:

$$\xi_i = \begin{cases} (a_{\parallel})^m(a_{\perp})^n(\rho_{roughness})^{m+n} \\ (a_{\perp})^m(a_{\parallel})^n(\rho_{roughness})^{m+n} \end{cases} \tag{24}$$

By defining the normalized direction function and direction coefficient of the antenna, the fading model of the coal mine RIS can be obtained. Suppose that the RIS is placed in the x-y plane of the Cartesian coordinate system facing the base station as shown in Figure 3, and the unit size of each RIS is $d_x \times d_y$, and $d_x = d_y = \lambda/2$. $R(p,q)$ is the RIS unit in row p with q columns, and each RIS unit has a programmable reflection coefficient, which is denoted as $\Gamma_{p,q}$, $p \in [1-\sqrt{N}/2, \sqrt{N}/2]$, $q \in [1-\sqrt{N}/2, \sqrt{N}/2]$.

Suppose that $L^{BS-RIS}_{m,p,q}$ represents the propagation distance of the mth antenna from BS to cell $R(p,q)$ of the RIS, and $L^{RIS-UE}_{p,q}$ represents the propagation distance from cell $R(p,q)$ of the RIS to UE. $\theta^{Tx}_{m,p,q}, \varphi^{Tx}_{m,p,q}, \theta^{Rx}_{p,q}, \varphi^{Rx}_{p,q}$ are used to represent the pitch angle and azimuth angle from the BS to the RIS unit $R(p,q)$, the pitch angle and the azimuth angle from the UE to the RIS unit $R(p,q)$, respectively. Similarly, $\theta^{T}_{m,p,q}, \varphi^{T}_{m,p,q}, \theta^{R}_{p,q}, \varphi^{R}_{p,q}$ represents the pitch and azimuth angles of the RIS unit $R(p,q)$ to the BS and UE, respectively. The specific representation can be seen in Figure 5 below.

To reduce interference and enhance signal strength in specific directions, the antenna is designed to radiate maximum power only within a certain directional range, while radiating little to no power in other directions. If the radiation field in space is considered, then the antenna's normalized directional function can be expressed as [22]:

$$F(\theta,\varphi) = \begin{cases} \cos^3\theta & \theta \in [0,\pi/2], \varphi \in [0,\pi/2] \\ 0 & \theta \in (0,\pi/2], \varphi \in [0,\pi/2] \end{cases} \tag{25}$$

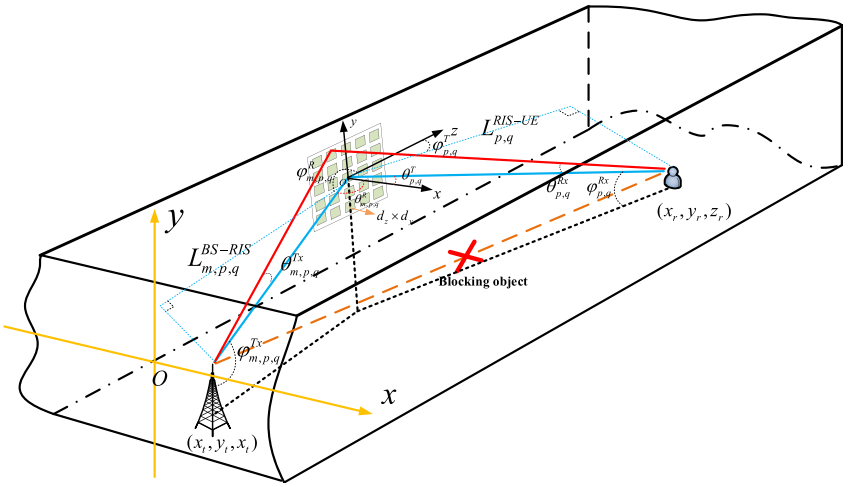

FIGURE 5. RIS-assisted communication beam pattern.

The orientation coefficient of the antenna is expressed as:

$$G = \frac{4\pi}{\int_{\varphi=0}^{2\pi}\int_{\theta=0}^{\pi} F(\theta,\varphi)\sin\theta d\theta d\varphi} \tag{26}$$

Assuming that the amplitude of all the reflective elements of the RIS is the same, it is denoted as A, but the phase shift is different, denoted as $\varphi_{p,q}$. In the RIS-assisted cascaded channel, the loss multiplication of the two links is considered. This means that the attenuation of the first segment path affects the initial power level for further attenuation on the second segment path. Then combined with Equation (22), the received signal power can be expressed as:

$$\begin{aligned} P_r = & \left| \sum_{i=1}^{M} \left[\sum_{p=1-\frac{\sqrt{N}}{2}}^{\frac{\sqrt{N}}{2}} \sum_{q=1-\frac{\sqrt{N}}{2}}^{\frac{\sqrt{N}}{2}} \sqrt{F^{combine}_{m,p,q}} \right.\right. \\ & \left.\left. \left(\sum_{j=1}^{R_{br}} \prod_{k=1}^{i} \xi_{ijk} \frac{\exp(-j\varphi_{ijk} + j\varphi_{p,q})}{L^{BS-RIS}_{i,j,p,q} \times L^{RIS-UE}_{p,q}} \right) \right] \right|^2 \\ & \times \left(\frac{P_t \lambda^4 G_t G_r G_0 N A (d_x d_y) \Psi(r)}{256\pi^3} \right) \end{aligned} \tag{27}$$

$$\begin{aligned} \sqrt{F^{combine}_{m,p,q}} = & F^{Tx}\left(\theta^{Tx}_{m,p,q}, \varphi^{Tx}_{m,p,q}\right) F\left(\theta^{T}_{p,q}, \varphi^{T}_{p,q}\right) \\ & \times F\left(\theta^{R}_{p,q}, \varphi^{R}_{p,q}\right) F^{Rx}\left(\theta^{Rx}_{m,p,q}, \varphi^{Rx}_{m,p,q}\right) \end{aligned} \tag{28}$$

Equation (28) represents the effect of the normalized directional function on the received power of the signal. Materializing the phase representation of Equation (27) yields:

$$\begin{aligned} P_r = & \left| \sum_{i=1}^{M} \left[\sum_{p=1-\frac{\sqrt{N}}{2}}^{\frac{\sqrt{N}}{2}} \sum_{q=1-\frac{\sqrt{N}}{2}}^{\frac{\sqrt{N}}{2}} \sqrt{F^{combine}_{m,p,q}} \right.\right. \\ & \left.\left. \left(\sum_{j=1}^{R_{br}} \prod_{k=1}^{i} \xi_{ijk} \frac{e^{\frac{-j\left(2\pi\left(L^{BS-RIS}_{i,j,p,q} + L^{RIS-UE}_{p,q}\right) - \lambda\varphi_{p,q}\right)}{\lambda}}}{L^{BS-RIS}_{i,j,p,q} \times L^{RIS-UE}_{p,q}} \right) \right] \right|^2 \\ & \times \left(\frac{P_t \lambda^4 N A G_t G_r G_0 (d_x d_y) \Psi(r)}{256\pi^3} \right) \end{aligned} \tag{29}$$

After the amplitude and phase modulation of RIS, when $\varphi_{p,q} = \varphi^{BS-RIS}_{i,j,p,q} + \varphi^{RIS-UE}_{p,q}$, the received power reaches the maximum value, so the optimal solution of Equation (29) is expressed as:

$$\begin{aligned} P_{r\max} = & \left| \sum_{i=1}^{M} \left[\sum_{p=1-\frac{\sqrt{N}}{2}}^{\frac{\sqrt{N}}{2}} \right.\right. \\ & \left.\left. \sum_{q=1-\frac{\sqrt{N}}{2}}^{\frac{\sqrt{N}}{2}} \sqrt{F^{combine}_{m,p,q}} \left(\sum_{j=1}^{R_{br}} \prod_{k=1}^{i} \frac{\xi_{ijk}}{L^{BS-RIS}_{i,j,p,q} \times L^{RIS-UE}_{p,q}} \right) \right] \right|^2 \\ & \times \left(\frac{P \lambda^4 G_t G_r G_0 (d_x d_y) N A \Psi(r)}{256\pi^3} \right) \end{aligned} \tag{30}$$

where $\varphi_{n,m} = mod\left(\frac{2\pi\left(L^{BS-RIS}_{i,j,p,q} + L^{RIS-UE}_{p,q}\right)}{\lambda}, 2\pi\right)$.

In this case, the path loss of RIS-assisted the coal mine tunnel communication is expressed as follows:

$$\begin{aligned} PL = & \frac{256\pi^3}{\lambda^4 G_t G_r G_0 N (d_x d_y) A \Psi(r)} \\ & \times \frac{1}{\left| \sum_{i=1}^{M} \left[\sum_{p=1-\frac{\sqrt{N}}{2}}^{\frac{\sqrt{N}}{2}} \sum_{q=1-\frac{\sqrt{N}}{2}}^{\frac{\sqrt{N}}{2}} \sqrt{F^{combine}_{m,p,q}} \left(\sum_{j=1}^{R_{br}} \prod_{k=1}^{i} \frac{\xi_{ijk}}{L^{BS-RIS}_{i,j,p,q} \times L^{RIS-UE}_{p,q}} \right) \right] \right|^2} \end{aligned} \tag{31}$$

4. ANALYSIS OF SIMULATION RESULTS

In order to deeply analyze the loss model of the radio wave propagation channel assisted by RIS in the underground coal mine roadway, a series of related simulation experiments were carried out in this part of the study.

TABLE 1. Simulation parameter configuration.

Parameter	Value
Transmitted power P_t	30 dBm
Transmitter gain G_t	5 dBm
Receiver gain G_r	5 dBm
The distance between the BS and the sidewall of the tunnel h_T	4.5 m
The height of the tunnel H	6 m
The width of the tunnel W	5 m
The distance between the receiving end and the sidewall of the roadway h_R	2 m
Number of transmitting antennas M	64
Effective scattering paths R_{br}	128
Rayleigh fading loss depth σ^2	8
Vacuum permittivity	8.854×10^{-12}

TABLE 2. The data points for loss every 25 m interval.

Distance (m)	2.4 GHz RIS (dBm)	2.4 GHz No_RIS (dBm)	5.8 GHz RIS (dBm)	5.8 GHz No_RIS (dBm)	30 GHz RIS (dBm)	30 GHz No_RIS (dBm)
50	-Inf	27.36	-Inf	39.62	-Inf	56.89
75	5.45	31.56	28.99	47.49	49.64	53.86
100	16.07	37.96	30.54	44.84	58.01	58.04
125	17.64	38.38	38.42	51.58	64.63	63.52
150	28.79	49.25	36.44	49.33	65.68	64.30
175	26.69	47.21	42.45	55.39	70.71	69.38
200	25.62	46.33	41.42	54.56	71.77	70.64

The simulation model establishes a specific scenario of a rectangular mine tunnel, characterized primarily by high reflectivity and confined space. The transmitting antenna is positioned at a designated location within the Cartesian coordinate system, and the RIS is composed of a square reflector with multiple elements. To assess system performance and the reliability of analytical results, we employed the Monte Carlo simulation method. This method approximates the behavior of complex systems through repeated random sampling, thereby providing a statistically robust experimental environment. The specific parameters of the simulation experiment are outlined in Table 1, chosen to ensure the accuracy and representativeness of the results. Notably, given the 200-meter propagation distance and the significant amount of reflection, the direct signal is dominant, thus obviating the need to separately consider different polarized wave scenarios [18]. Furthermore, the simulation fixes the distance between the RIS and the BS at 50 meters. In the near-field region, the signal predominantly follows the Line-of-Sight (LOS) path from the BS, which is not discussed in detail. Here, the RIS serves primarily for blind zone coverage and extension of communication distance.

The results for experimental analysis of the radio wave propagation loss characteristic for the RIS fading channel in a coal mine tunnel are shown in Figure 6. Experiments were conducted using radio signal in the 2.4 GHz, 5.8 GHz, and 30 GHz frequency bands, with a transmission distance up to 200 m. The distance between the BS and the RIS panel was fixed at 50 m. The data sampling was conducted at intervals of 25 m, and the results are presented in Table 2. Combining the simulation images and the data, it can be concluded that at a transmission distance of 100 meters, the radio wave loss for the 2.4 GHz frequency band in the coal mine tunnel without RIS assistance is 37.96 dBm. The wave loss is reduced to 16.07 dBm if with the RIS assistance, a decrease of 21.89 dBm resulting in a reduction of loss by 54.78% and the transmission distance can

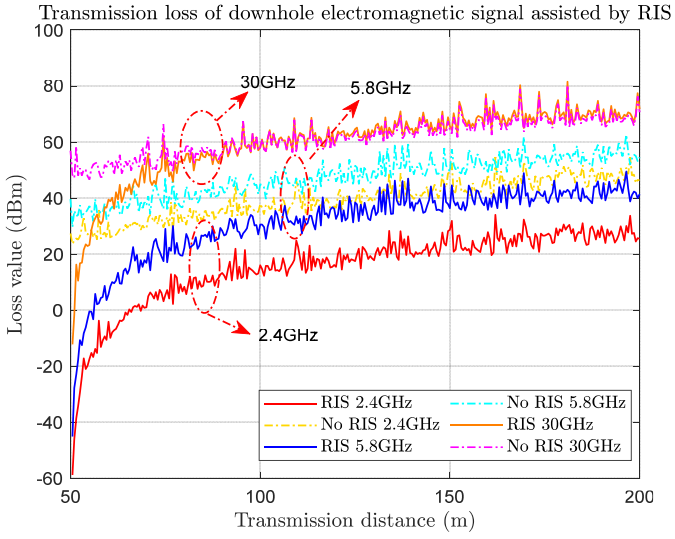

FIGURE 6. Comparison of downhole signal loss in the 2.4 GHz, 5.8 GHz and 30 GHz bands with or without RIS assistance.

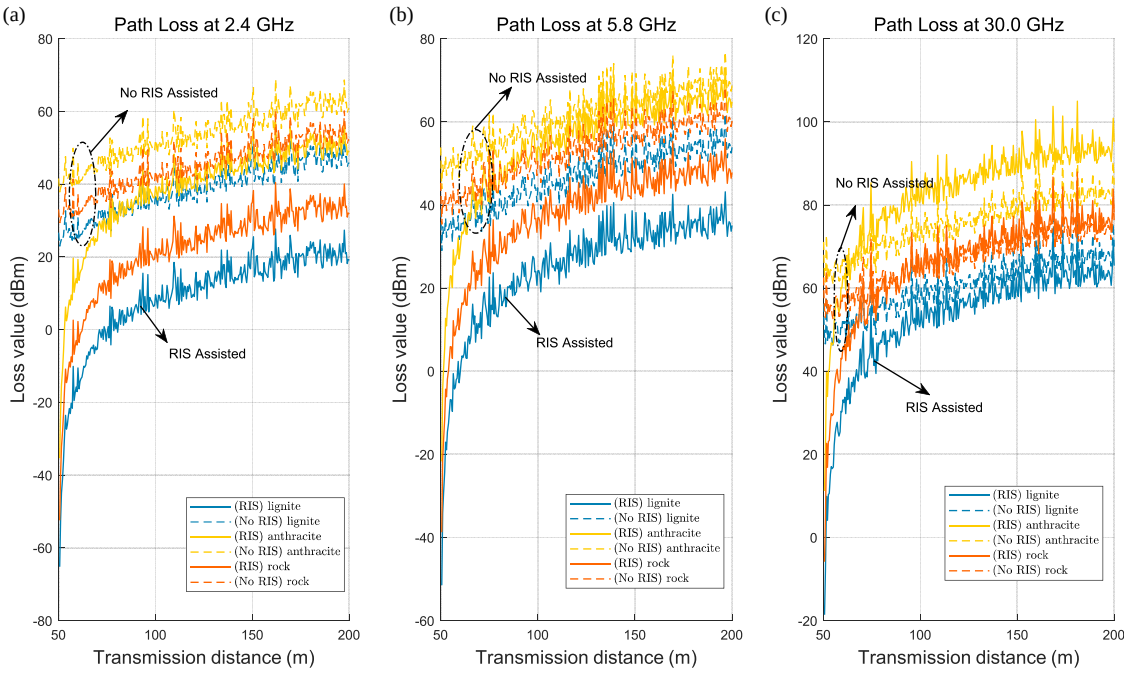

FIGURE 7. Loss characteristics of 2.4 GHz, 5.8 GHz, and 30 GHz frequency band signals in lignite, rock, and anthracite.

be increased by at least 236 meters compared with the signal propagation without RIS. When the transmission distance extends to 200 m, the observed radio wave loss in the coal mine tunnel without RIS assistance in the 2.4 GHz frequency band is 46.33 dBm. However, with the integration of RIS, this loss significantly decreases to 25.62 dBm, marking an improvement of 20.71 dBm. This translates to a substantial reduction in the loss of 44.70%. In a similar vein, at a transmission distance of 100 meters, the radio wave loss in the 5.8 GHz frequency band without RIS assistance is measured at 44.84 dBm. With the aid of RIS, this loss is mitigated to 30.54 dBm, a decrease of 14.30 dBm, resulting in a reduction of loss by 31.89%. At the same frequency band but at a distance of 200 m, the wave loss without RIS assistance is higher, at 54.56 dBm. RIS assistance brings this down to 41.42 dBm, an improvement of 13.14 dBm, reducing the loss by 24.08%.

These results highlight a key trend: as the distance from the RIS reflective surface increases, the radio wave loss incrementally rises, and the efficacy of RIS in mitigating this loss diminishes. Moreover, for high-frequency signals at 30 GHz, the beneficial impact of RIS on wave loss is modest, at just 0.05% improvement when the transmission distance is 100 meters. Beyond this distance, RIS does not significantly enhance signal performance. This suggests that low-frequency signals, particularly in the 2.4 GHz band, are more apt for underground communication networks. Such frequencies experience lower reflective losses in the coal mine tunnel alleyways, and RIS technology offers more pronounced improvements in signal propagation and reach for these lower frequencies. On the other hand, for high-frequency signals like 30 GHz millimeter-wave transmissions, deploying multiple RIS units in a cascaded arrangement could be considered for optimized signal propagation and enhanced coverage in blind spots. It should be noted that the model does not fully consider the low-band near-field model and only compares the 2.4 GHz signal with the 30 GHz signal, so there is a certain error in the simulation data, but the conclusions are somewhat illustrative.

In order to study the influence of different coal seams on the propagation signal, the loss simulation comparison of coal seams with different dielectric constants is shown in Figure 7. The experiment focused on rock, lignite, and anthracite. The parameter settings were similar to those in Figure 5, with the RIS dimension being 40×40 and each RIS element sized at $d_x = d_y = \lambda/2$. The signal measurement distance was set at 200 meters. The dielectric constant of coal rock is related to the propagation frequency and gradually decreases with the increase of frequency. Here, three typical dielectric layers are considered, namely lignite seams, anthracite seams, and clay seams (rocks). In general, the relative permittivity of lignite is greater than that of anthracite and clay, because lignite contains more water and organic matter. In contrast, most rock types (e.g., sandstone, limestone, granite, etc.) typically have a low relative permittivity (generally between 2–12). In the experiment, the relative permittivity of lignite is 25; the dielectric constant of anthracite is 4.5; and the dielectric constant of clay is 12. The data clearly indicates that for high-frequency 30 GHz signals, regardless of the coal rock material, the electrical signal loss remains significantly higher than that of lower-frequency signals.

Taking the distance of three different signal frequencies to 100 meters as an example, the 2.4 GHz signal loss through lignite is 33.52 dBm, 48.42 dBm through anthracite, and 43.65 dBm through rock without RIS assistance. For the 5.8 GHz signal, the corresponding loss is 44.07 dBm in lignite, 62.71 dBm in anthracite, and 54.19 dBm in rock. For the 30 GHz signal, the corresponding loss is 63.87 dBm for

TABLE 3. The received power data points at intervals of 25 m for three sizes of RIS panels.

	2.4 GHz_RIS Size			5.8 GHz_RIS Size			30 GHz_RIS Size		
Distance (m)	40×40	60×60	80×80	40×40	60×60	80×80	40×40	60×60	80×80
50	Inf	Inf	Inf	Inf	Inf	Inf	Inf	Inf	Inf
75	18.15	25.20	30.19	−5.48	1.55	6.55	−26.09	−19.05	−14.05
100	5.19	12.24	17.23	−9.39	−2.34	2.64	−36.82	−29.78	−24.78
125	1.51	8.55	13.55	−19.39	−12.35	−7.35	−45.57	−38.53	−33.53
150	−11.38	−4.34	0.65	−19.16	−12.12	−7.12	−48.38	−41.33	−36.33
175	−10.75	−3.70	1.28	−26.64	−19.59	−14.60	−54.87	−47.83	−42.83
200	−10.94	−3.89	1.09	−26.87	−19.83	−14.83	−57.19	−50.15	−45.15

lignite, 81.61 dBm for anthracite, and 64.85 dBm in rock. The experimental data show that the loss is relatively low for the lignite with high dielectric coefficient at the same frequency, but relatively large for anthracite with low dielectric constant. Because in the short transmission of 200 meters, the high reflection causes the high conductivity material to reflect the signal more than to absorb it, so the signal at the receiving end will be relatively large.

In addition, from the perspective of RIS improvement, the addition of RIS has a significant improvement effect on the attenuation signals of different coal seams. This improvement is more pronounced for low-frequency signals, resulting in a longer effective propagation distance. For the 30 GHz signal, if the coal seam is anthracite, when the transmission reaches a distance about 70 meters, the improvement of RIS is not obvious, so for the anthracite mining, the collaborative optimization of multiple RISs is mainly considered to expand the propagation range of the signal.

Furthermore, RIS-assisted channels show a notable improvement in loss for coal layers with different dielectric constants,

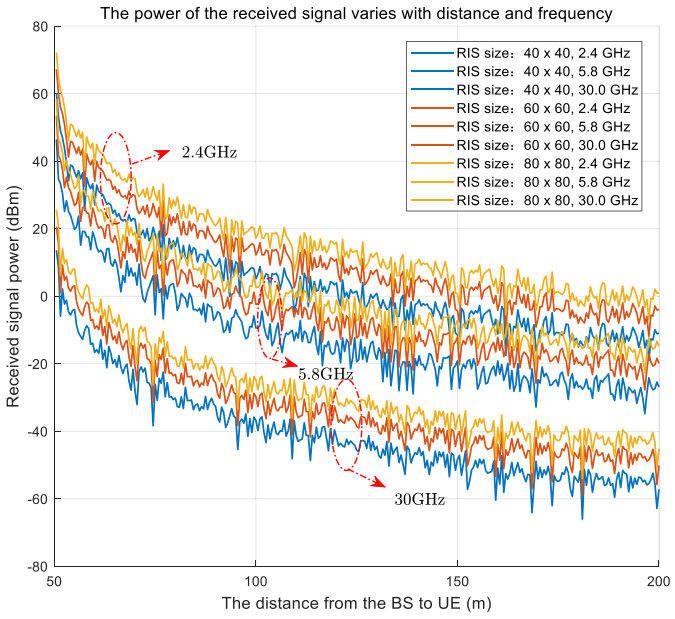

FIGURE 8. The impact of RIS size on received signal power and received power values at 25 m intervals under different RIS sizes.

demonstrating the feasibility and effectiveness of RIS in underground signal propagation.

According to the relationship between different RIS sizes and the user's received power, simulation experiments are carried out in Figure 8. Correspondingly, the data points at 25-meter intervals for the three RIS sizes are shown in Table 3. Three RIS panels of different sizes were used, with element numbers of 40×40, 60×60, and 80×80. The experiment tested the power of received signals within a 200 meters transmission distance, under a constant transmission power of 30 dBm. The results demonstrate that larger RIS panels can effectively enhance the signal power at the receiver's end. In other words, under the same receiving power conditions within a given frequency band, a larger RIS can transmit signals over a greater distance. For instance, in the 2.4 GHz frequency band, with a fixed receiving power of 20 dBm, the 40×40 RIS panel can propagate the signal to approximately 70 meters; the 60×60 panel can reach around 85 meters, and the 80×80 panel can extend to about 100 meters. Similarly, for lower frequency signals, larger RIS panels can transmit over even longer distances.

Taking 100 meters as a testing point, for a 30 GHz signal, the 40×40 RIS array received a signal strength of -36.82 dBm at this distance. In comparison, a 60×60 RIS array at the same frequency received a signal power of -29.78 dBm, and the 80×80 RIS array received -24.78 dBm. As the size of the RIS increases, the power of the received signal progressively increases. Therefore, for underground communications, it is advisable to consider using larger-sized RIS panels in the 2.4 GHz frequency band. However, it is important to note the limitations posed by the confined space within tunnels; RIS cannot be infinitely large. Additionally, the gain coefficient of each reflective element should be considered to ensure safety within the coal mine tunnel.

5. CONCLUSION

This study delves into the application of large-scale Reflective Intelligent Surface (RIS) technology in underground coal mine environments to enhance the efficacy of downlink signal reception for users. Through a detailed examination of the far-field characteristics of RIS, this paper reveals the profound impact of the complex coal mine underground environment on the properties of radio wave transmission. The findings demonstrate that the use of large-scale RIS significantly improves signal quality and effectively augments coverage in signal blind spots. In

addition, this study thoroughly analyzes the RIS-assisted radio wave transmission mechanism, including an in-depth investigation of the reflection, refraction, and scattering processes of radio waves. Theoretical analyses and simulation experiments jointly confirm the substantial advantages of RIS technology in expanding signal coverage and enhancing transmission efficiency. Moreover, compared to traditional communication systems, RIS-assisted communication systems exhibit significant superiority in improving communication efficiency.

ACKNOWLEDGEMENT

This work was supported by the National Natural Science Foundation of China (NSFC52174197): The extraction and quantitative recognition of UWB radar vital information features for mine borehole rescue.

REFERENCES

[1] "IMT-2030 (6G) Promotion Group officially released the White Paper "6G Overall Vision and Potential Key Technologies"," *White Paper*, Vol. 6, 8–9C, 2021.

[2] Huang, C., A. Zappone, G. C. Alexandropoulos, M. Debbah, and C. Yuen, "Reconfigurable intelligent surfaces for energy efficiency in wireless communication," *IEEE Transactions on Wireless Communications*, Vol. 18, No. 8, 4157–4170, Aug. 2019.

[3] He, J., H. Wymeersch, T. Sanguanpuak, O. Silven, and M. Juntti, "Adaptive beamforming design for mmWave RIS-aided joint localization and communication," in *2020 IEEE Wireless Communications and Networking Conference Workshops (WCNCW)*, 1–6, Seoul, Korea (South), 2020.

[4] Cui, T. J., M. Q. Qi, X. Wan, J. Zhao, and Q. Cheng, "Coding metamaterials, digital metamaterials and programmable metamaterials," *Light: Science & Applications*, Vol. 3, e218, 2014.

[5] Wu, Q. and R. Zhang, "Towards smart and reconfigurable environment: Intelligent reflecting surface aided wireless network," *IEEE Communications Magazine*, Vol. 58, No. 1, 106–112, Jan. 2020.

[6] Jung, M., W. Saad, M. Debbah, and C. S. Hong, "On the optimality of reconfigurable intelligent surfaces (RISs): Passive beamforming, modulation, and resource allocation," *IEEE Transactions on Wireless Communications*, Vol. 20, No. 7, 4347–4363, Jul. 2021.

[7] Huang, C., A. Zappone, G. C. Alexandropoulos, M. Debbah, and C. Yuen, "Reconfigurable intelligent surfaces for energy efficiency in wireless communication," *IEEE Transactions on Wireless Communications*, Vol. 18, No. 8, 4157–4170, Aug. 2019.

[8] Jung, M., W. Saad, Y. Jang, G. Kong, and S. Choi, "Reliability analysis of large intelligent surfaces (LISs): Rate distribution and outage probability," *IEEE Wireless Communications Letters*, Vol. 8, No. 6, 1662–1666, Dec. 2019.

[9] Kilinc, F., I. Yildirim, and E. Basar, "Physical channel modeling for RIS-empowered wireless networks in sub-6 GHz bands," in *2021 55th Asilomar Conference on Signals, Systems, and Computers*, 704–708, Pacific Grove, CA, USA, 2021.

[10] Sang, J., M. Zhou, J. Lan, B. Gao, W. Tang, X. Li, S. Jin, E. Basar, C. Li, Q. Cheng, and T. J. Cui, "Multi-scenario broadband channel measurement and modeling for sub-6 GHz RIS-assisted wireless communication systems," *ArXiv abs/2305.07835*, 2023.

[11] He, Z.-Q. and X. Yuan, "Cascaded channel estimation for large intelligent metasurface assisted massive MIMO," *IEEE Wireless Communications Letters*, Vol. 9, No. 2, 210–214, Feb. 2020.

[12] Zheng, B. and R. Zhang, "Intelligent reflecting surface-enhanced OFDM: Channel estimation and reflection optimization," *IEEE Wireless Communications Letters*, Vol. 9, No. 4, 518–522, Apr. 2020.

[13] He, J., N. T. Nguyen, R. Schroeder, V. Tapio, J. Kokkoniemi, and M. Juntti, "Channel estimation and hybrid architectures for RIS-assisted communications," in *2021 Joint European Conference on Networks and Communications & 6G Summit (EuCNC/6G Summit)*, 60–65, Porto, Portugal, Jun. 2021.

[14] Zappone, A., M. D. Renzo, F. Shams, X. Qian, and M. Debbah, "Overhead-aware design of reconfigurable intelligent surfaces in smart radio environments," *IEEE Transactions on Wireless Communications*, Vol. 20, No. 1, 126–141, Jan. 2021.

[15] Xiong, R., J. Zhang, F. Wang, *et al.*, "A review of intelligent metasurface design in wireless communication," *Journal of Huazhong University of Scienceand Technology (Natural Science Edition)*, Vol. 51, No. 9, 2023.

[16] Li, S., Z. Peng, M. Min *et al.*, "Discussion on intelligent reflecting surface technology and its application in wireless blind spot coverage in coal mines," *Journal of Mine Automation*, Vol. 49, No. 6, 112–119, 2023.

[17] Zheng, H., X. Zhao, X. Nie, *et al.*, "Research on MIMO channel model in coal mine," *Journal of Mine Automation*, Vol. 35, No. 8, 2009.

[18] Wang, S., F. Tao, and Z. Guo, "Study of radio wave propagation characteristics from sources at different locations in a mine," *Coal Technology*, Vol. 29, No. 3, 186–188, 2010.

[19] Emslie, A., R. Lagace, and P. Strong, "Theory of the propagation of UHF radio waves in coal mine tunnels," *IEEE Transactions on Antennas and Propagation*, Vol. 23, No. 2, 192–205, Mar. 1975.

[20] Zheng, H., "Research on the theory of radio wave propagation and key technology of MIMO channel modeling in coal mine roadway," Ph.D. dissertation, China University of Mining and Technology, 2010.

[21] Zhang, H., H. Yu, W. Pu, *et al.*, "Establishment and simulation of radio wave multipath propagation model in rectangular tunnel," *Chinese Journal of Radio Science*, 195–200, 2008.

[22] Tang, W., M. Z. Chen, X. Chen, J. Y. Dai, Y. Han, M. D. Renzo, Y. Zeng, S. Jin, Q. Cheng, and T. J. Cui, "Wireless communications with reconfigurable intelligent surface: Path loss modeling and experimental measurement," *IEEE Transactions on Wireless Communications*, Vol. 20, No. 1, 421–439, Jan. 2021.